IEEE Access
Multidisciplinary | Rapid Review | Open Access Journal

Received June 16, 2021, accepted July 3, 2021, date of publication July 9, 2021, date of current version July 20, 2021.

Digital Object Identifier 10.1109/ACCESS.2021.3095852

RIS-Aided Physical Layer Security With Full-Duplex Jamming in Underlay D2D Networks

WAQAS KHALID[1], HEEJUNG YU[2], (Senior Member, IEEE), DINH-THUAN DO[3], (Senior Member, IEEE), ZEESHAN KALEEM[4], (Senior Member, IEEE), AND SONG NOH[5], (Member, IEEE)

[1]Institute of Industrial Technology, Korea University, Sejong 30019, South Korea
[2]Department of Electronics and Information Engineering, Korea University, Sejong 30019, South Korea
[3]Department of Computer Science and Information Engineering, Asia University, Taichung 41354, Taiwan
[4]Department of Electrical and Computer Engineering, COMSATS University Islamabad, Wah Campus 47040, Pakistan
[5]Department of Information and Telecommunication Engineering, Incheon National University, Incheon 22012, South Korea

Corresponding authors: Heejung Yu (heejungyu@korea.ac.kr) and Song Noh (songnoh@inu.ac.kr)

This work was supported in part by the National Research Foundation of Korea (NRF) Grant through the Ministry of Science and ICT (MSIT), South Korea under Grant 2019R1A2C1083988, in part by the Basic Science Research Program through the NRF funded by the Ministry of Education under Grant 2021R1I1A3041887, and in part by the MSIT, South Korea, through the Information Technology Research Center (ITRC) Support Program supervised by the Institute for Information and communications Technology Promotion (IITP) under Grant IITP-2021-2016-0-00313.

ABSTRACT This paper investigates the physical layer security and data transmission for the underlay device-to-device (D2D) networks, and considers a combination of the reconfigurable intelligent surface (RIS) and full-duplex (FD) jamming receiver for the robustness and security enhancements of the system. In the demonstrated spectrum sharing setup, the total power of the D2D networks is conceived to the transmitter and receiver to transmit a private message and emit the artificial noise (AN) signals. To prevent information leakage, a beamforming design is presented for a multi-antenna FD D2D receiver in order to suppress and inject the AN signals in the direction of legitimate users and eavesdropper, respectively. The statistical characterization of end-to-end RIS-assisted wireless channels is presented, and the achievable ergodic secrecy rate of the system is derived in novel approximate expressions. The numerical and simulation results confirm the accuracy and effectiveness of the proposed analytical framework. The results demonstrate an optimal selection of the D2D power allocations for different number of reflecting elements in terms of achievable ergodic secrecy rates of the system.

INDEX TERMS Underlay D2D networks, reconfigurable intelligent surface, full-duplex jamming, ergodic secrecy rates.

I. INTRODUCTION

Over the past few years, the revolutionary progress in wireless communication protocols, computing capabilities, and sensors has enabled a new technology paradigm, i.e., Internet of Things (IoT). The major applications of IoT include healthcare, smart surveillance, automated transportation, industrial automation, remote management, and extended reality reality [1]. The global mobile traffic volume and internet-connected smart devices by 2030 are expected to exceed 5016 Exabyte/month, and 40 billion, respectively. However, the scarcity of spectrum resources is a challenge in establishing the ubiquitous connectivity, bandwidth demands, and optimized support for IoT; thus, identifying the novel enabling technologies and wireless communication networks is a necessity [2], [3]. Fifth generation (5G) networks are expected to play a key role in the widespread adoption of IoT. The standardization activities and deployment of 5G networks enabling the advanced functions such as ultra reliability, low latency, and mass connectivity have begun worldwide. The potential enabling technologies of 5G include multiple-input multiple-output (MIMO) [4], non-orthogonal multiple access (NOMA) [4], ultra-dense small cells [5], millimeter wave (mmWave) communication [5], and software-defined cognitive radios [6]. Despite the potential of these revolutionary technologies, 5G cannot

The associate editor coordinating the review of this manuscript and approving it for publication was Young Jin Chun.

meet all the requirements of a post-2030 world. Therefore, the conceptualization of the sixth generation (6G) networks has been started.

The core requirements, service categories, and enabling technologies of 6G networks present an interesting future of wireless communications [7], [8]. To derive the actualization of 6G networks, massive MIMO [9], artificial intelligence (AI) [10], efficient spectrum sharing [11], full-duplex (FD) communication [12], and reconfigurable intelligent surface (RIS) [13] are the potential key enabling technologies and solutions. In particular, RIS is a revolutionizing technology which reconfigures the wireless propagation environment smartly via software-controlled reflections. In a detail, passive reflecting elements integrated on a planar surface reflect the incident signals independently by controlling the amplitudes and/or phases, thereby collectively achieving a high-precision beamforming to enhance or cancel signals in any direction. Consequently, RIS improves the link performance and ensures a reliable reception. The advantages of RIS include high flexibility, superior compatibility, and low-cost deployment, and the design challenges include channel acquisition, beamforming design, and optimization [14].

In other developments, the security-sensitive applications require hyper-secured wireless networks. The private data are susceptible to malicious overhearing attacks owing to the broadcast nature of the wireless signals. The assurance of data security from the application to physical layers is essential. In this regard, the information-theoretic physical layer security (PLS) provides security against unintended users/eavesdroppers and ensures the data confidentiality. PLS limits the signal-to-interference-plus-noise ratio (SINR) to the eavesdroppers by utilizing the physical characteristics of the wireless channels, and enables the signals to be decoded at the intended users only. Eavesdroppers are classified into two complementary categories: passive eavesdroppers, who attempt to decode/analyze the information, and active eavesdroppers, who attempt to alter the information. In general, secrecy rate is considered as a optimization objective for the security provisioning [15], [16].

A. RELATED WORK

Several techniques have been investigated to improve the spectrum utilization and fulfill the massive connectivity demands [17]–[20]. For example, FD communications improve the spectral efficiency. Particularly, the recent advances in self-interference (SI) cancellation have made FD a practical choice for the wireless applications [17]. The sharing of spectral resources of the cellular networks with D2D users is another approach to reuse the spectrum. The D2D communications offload the cellular traffic, deliver the content directly among proximity users, and offer the advantages, including reduced transmission latency, extended cellular coverage, and enhanced spectral/energy efficiency [18], [19]. The integration of FD in D2D communications provides an efficient design solution for the network architecture of 6G networks [20]. However, the potential gain of the cellular networks with underlay FD D2D communications requires efficient interference management and resource allocation. It is important to design efficient spectrum-sharing schemes to improve the cellular and D2D links simultaneously.

Simultaneously, academia and industry have shown tremendous interest to unlock the superior advantages of RIS, and enhance the several performance metrics of the networks, such as sum-secrecy rates, energy efficiency, and spectral efficiency. Different application scenarios of RIS have been introduced, including device-to-device (D2D) communication [21], mmWave communication [22], coordinated multipoint (CoMP) transmission [23], simultaneous wireless information and power transfer (SWIPT) [24], and PLS [25]–[27]. In specific to PLS, [25] adjusted the phase shifts and transmit powers to enhance the PLS performance in RIS-assisted two-way communications. The authors in [26] presented the secrecy maximization problem in RIS-assisted multiuser two-way communications by utilizing the signals of the users for degrading the eavesdropping capability. Moreover in [27], the proposed RIS-based channel randomization technique improved the secrecy performance for a downlink cellular wire-tap network. The application of PLS was also extended to the D2D communications underlaying cellular networks where the system interference was utilized to enhance the secrecy performance [28], [29]. Such a scenario provided a win-win situation as each node simultaneously achieved its own transmission. In contrast, friendly jammers required power to interfere with the malicious users [30]. The underlay FD D2D networks also improved the security of the system. The FD D2D receiver simultaneously received the confidential signal using the SI elimination procedure and generated the jamming signals to confuse the eavesdropper [31].

B. MOTIVATION, NOVELTY AND CONTRIBUTION

To summarize, the efficient spectrum sharing for underlay D2D networks with the performance enhancements via RIS, FD radios, and PLS, is required for the 6G era. In general, underlay D2D networks were analyzed in a typical setting of the spectrum sharing, i.e., a D2D transmitter secured the cellular network via jamming signals, using either a relay or a direct link [32]. The requirement of a power source and the negative impact of additive noise do not make relays a good choice for the poor-quality users [33]. The direct link and proximity conditions also do not guarantee a reliable transmission. Consequently, the integration of RISs with underlay D2D networks is essential. In addition, a secure D2D communication in underlay networks has become a prerequisite, as security issues have become a major concern, particularly with the IoT developments [34]. The combined application of the RIS and FD jamming receivers can be useful for the robustness and security enhancements of overall underlay networks. Existing literature does not focus on the above-mentioned work and bridging these gaps is the motivation behind our work.

This paper presents a theoretical framework to quantify the robustness and security performance of RIS-assisted underlay D2D networks. An interesting application scenario is developed by introducing a multi-antenna D2D receiver as a FD jamming receiver. Consequently, the D2D transmitter and receiver share the total power, to transmit and emit the confidential and jamming signals, respectively. Finally, the optimal D2D power allocations according to number of reflecting elements for the achievable ergodic secrecy rates are identified. The technical contribution of this paper is:

- Novel system setting: Presenting a novel analytical framework of spectrum sharing for RIS-assisted underlay D2D networks, the robustness and security enhancements of the system are investigated using a combination of the RIS and FD jamming receiver. To facilitate the stringent quality-of-service (QoS) requirements in cellular network, both direct and RIS cascaded links are considered. In our setup, a D2D receiver selects an antenna for the maximum reception, and beamforming is designed for the remaining antennas to inject and suppress the artificial noise (AN) in the direction of eavesdropper and legitimate users, respectively.
- Performance analysis: The statistical characterization of the end-to-end (E2E) RIS-assisted wireless channels and instantaneous E2E SINRs is presented. Building upon these expressions, the approximate expressions of the achievable ergodic secrecy rates of the system are derived. In particular, the effective channel powers for the legitimate receivers are approximated with the gamma distribution using moment-matching technique. In contrast, the exponential and hypoexponential distributions are considered for the eavesdropping links.
- Insightful observations: Numerical results confirm an agreement between the theoretical and simulation results. The results suggest an optimization of D2D power allocations for the achievable ergodic secrecy rates of the system and provide valuable insights for an optimal selection with respect to number of reflecting elements.

C. NOTATIONS AND PAPER ORGANIZATION

Notation: In this paper, vectors and matrices are shown in bold letters. $\mathbf{x}^H$, $\|\mathbf{x}\|$, and $\mathbf{x}^{-1}$ denote the Hermitian transpose, Euclidian norm, and inverse operators of a matrix $\mathbf{x}$, respectively. $[\mathbf{x}]_z$ and $|.|$ implies the z element of $\mathbf{x}$ and the absolute value, respectively. arg (x) returns the argument of a complex number x and diag $\{\mathbf{x}\}$ denotes a diagonal matrix in which each diagonal element is the corresponding element in $\mathbf{x}$. The space of $P \times Q$ complex-valued matrices is denoted by $\mathcal{C}^{\mathcal{P}\times\mathcal{Q}}$. The symbols $\dot{\sim}$ and $\odot$ mean approximately follow the distribution and element-wise product, respectively. $\mathbb{E}\{.\}$, $\mathbb{V}\{.\}$, f_X and F_X denote the statistical expectation, variance, probability density function (PDF) and cumulative distribution function (CDF) of a random variable ($\mathcal{RV}$), respectively. log $(.)$ and ln $(.)$ stand for the binary and natural logarithm functions, respectively. Furthermore, $K_v(.)$ stands for the modified Bessel function of the second kind.

TABLE 1. List of abbreviations.

Abbreviation	Description
D2D	Device-to-device
RIS	Reconfigurable intelligent surface
FD	Full-duplex
AN	Artificial noise
IoT	Internet of Things
5G	The fifth generation
MIMO	Multiple-input multiple-output
NOMA	Non-orthogonal multiple access
mmWave	Millimeter wave
6G	The sixth generation
AI	Artificial intelligence
PLS	Physical layer security
SINR	Signal-to-interference-plus-noise-ratio
SI	Self-interference
CoMP	Coordinated multipoint
SWIPT	Simultaneous wireless information and power transfer
QoS	Quality-of-service
E2E	End-to-end
PDF	Probability density function
CDF	Cumulative distribution function
CSI	Channel state information
LoS	Line-of-sight
AWGN	Additive white Gaussian noise

The rest of this paper is organized as follows: In Section II, the system model of the presented framework, including the network description, design of beamforming and AN, and signal transmission model, is provided. Section III describes the analytical framework of the statistical characterization of RIS-assisted E2E wireless channels, and Section IV presents the achievable ergodic secrecy rate analysis. Section V reports the numerical results to validate the analytical results with the performance comparison. Finally, the conclusions of the paper are summarized in Section VI.

The abbreviations and notations used in this paper are listed in Tables 1 and 2, respectively.

II. SYSTEM MODEL

A. NETWORK DESCRIPTION

As shown in Fig. 1, a spectrum sharing setup for a cellular network with in-band underlay D2D communications is considered. The D2D users transmit simultaneously in the same spectral band, and in a compensation, contribute to a high-level security of the system [33], [34]. In the downlink transmission scenario, a D2D transmitter (DT) and a cellular base station (CT) send information symbols to a D2D receiver (DR) and a cellular user (CR), respectively, under the malicious attempt of a passive eavesdropper (E). To assist the transmissions and improve the instantaneous SINR at the intended receivers, RISs are deployed, i.e., RiS_c in the vicinity of CT, and RiS_d in the vicinity of DT. To facilitate the high SINR requirements for a CR, both the direct and RIS-cascaded links are considered. A RIS-cascaded without a direct link is considered for a D2D user. For analysis, the transmission mode of all nodes other than DR is set as a half-duplex with a single-antenna. In contrast, DR with

TABLE 2. List of notations.

Notation	Description
RiS_c	RIS in cellular network
RiS_d	RIS in D2D network
M	Number of antennas at DR
R	Number of reflecting elements of RiS_c
S	Number of reflecting elements of RiS_d
φ	Ratio of D2D power allocation
$\boldsymbol{\Upsilon}$	Vector of AN signals
$\boldsymbol{\Omega}$	Beamforming matrix
$\boldsymbol{\Theta}_c$	Phase shift matrix of RiS_c
$\boldsymbol{\Theta}_d$	Phase shift matrix of RiS_d
n_i	AWGN at i receiver
σ_i^2	Variance of AWGN at i receiver
b_{sic}	SI elimination factor
γ_L^C	SINR at CR
γ_L^D	SINR at DR
γ_E^C	SINR to decode cellular symbol at E
γ_E^D	SINR to decode D2D symbol at E
Λ_c	Effective channel power for CR
Λ_d	Effective channel power for DR
R_L^C	Achievable ergodic rate at CR
R_L^D	Achievable ergodic rate at DR
R_E^C	Achievable ergodic rate of cellular symbol at E
R_E^D	Achievable ergodic rate of D2D symbol at E

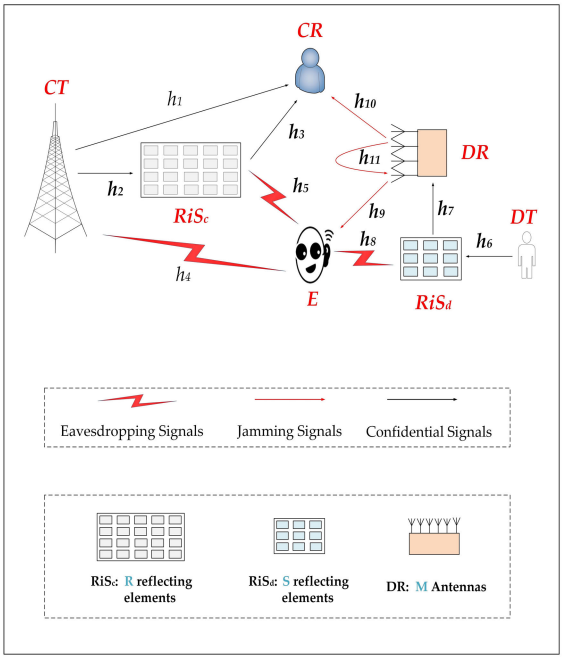

FIGURE 1. System model.

M antennas in a multi-antenna setup works in a FD mode. DR selects an antenna for the maximum reception from RiS_d, and designs the beamforming to use $M-1$ antennas to emit the AN signals in the direction of E[1] and suppress the AN signals in the directions of CR and receiving antenna of DR.[2]

[1]The jamming signals for E are provided via direct link only because a scenario is considered where the direct distance between E and DR is significantly smaller than via RiS_d.

[2]Due to the proximity of the D2D users, the signal from RiS_c to DR is not included. However, in practice, CT is unaware of the D2D transmissions in underlay D2D networks. The changing in this setting will provide a more general system setup and has been left for future work.

The conventional RIS setup, i.e., a planar surface with several passive reflecting elements and a smart controller, is considered [35]. To demonstrate the practical setup of RIS-assisted underlay networks and examine the impact of the reflecting elements precisely, different number of reflecting elements is considered in both networks. In particular, RiS_c and RiS_d contain R and S number of reflecting elements, respectively, and adjust their phase shifts to constructively add the signals at CR and DR, respectively.

Without loss of generality, all the baseband equivalent channels are assumed to be independent, identical, and flat, with the amplitudes following the Rayleigh distribution[3] with a scale parameter equal to 1.[4] In total, there are 11 communication links, $CT \rightarrow CR$, $C \rightarrow RiS_c$, $RiS_c \rightarrow CR$, $CT \rightarrow E$, $RiS_c \rightarrow E$, $DT \rightarrow RiS_d$, $RiS_d \rightarrow DR$, $RiS_d \rightarrow E$, $DR \rightarrow E$, $DR \rightarrow CR$, and $DR \rightarrow DR$, and are denoted by the complex channel coefficients, $h_1 \in \mathbb{C}$, $\mathbf{h}_2 \in \mathbb{C}^{R\times 1}$, $\mathbf{h}_3 \in \mathbb{C}^{R\times 1}$, $h_4 \in \mathbb{C}$, $\mathbf{h}_5 \in \mathbb{C}^{R\times 1}$, $\mathbf{h}_6 \in \mathbb{C}^{S\times 1}$, $\mathbf{h}_7 \in \mathbb{C}^{S\times 1}$, $\mathbf{h}_8 \in \mathbb{C}^{S\times 1}$, $\mathbf{h}_9 \in \mathbb{C}^{(M-1)\times 1}$, $\mathbf{h}_{10} \in \mathbb{C}^{(M-1)\times 1}$, and $\mathbf{h}_{11} \in \mathbb{C}^{(M-1)\times 1}$, respectively.

B. DESIGN OF BEAMFORMING AND AN

First, a DR selects an antenna as $\arg\max_{m=1,\cdots,M} |\Lambda_{dm}|^2$ to maximize the received power, where $|\Lambda_{dm}|^2$ is the effective channel power from the DT to the antenna m at DR. Conceiving the total power of D2D networks is P_d, in which, a portion of P_d, φ, is assigned to DT to transmit the confidential information symbol to DR, and the remaining portion, $1-\varphi$, is used by DR to emit the AN signals to E, where $0 \leq \varphi \leq 1$ is the ratio of the D2D power allocation.[5] Υ is a $(M-1)\times 1$ Gaussian vector of the AN signals having all the element entities with a zero mean and unit variance. Because the CSI of E is unknown, the power $(1-\varphi)P_d$ is allocated evenly to $M-1$ entities of Υ to emit the AN signal. To protect the DR and CR against the AN signals, an $(M-1)\times(M-1)$ beamforming matrix, Ω, is designed as

$$\Omega = \frac{\mathbf{I}_{M-1} - \mathbf{Q}}{\|\mathbf{I}_{M-1} - \mathbf{Q}\|}, \tag{1}$$

where $\mathbf{Q}$ is given by $\widehat{\mathbf{O}}(\widehat{\mathbf{O}}^H\widehat{\mathbf{O}})^{-1}\widehat{\mathbf{O}}^H$. $\mathbf{I}_{M-1}$ is an $(M-1)\times(M-1)$ identity matrix, and $\widehat{\mathbf{O}}$ is defined as $[\mathbf{h}_{10}\ \mathbf{h}_{11}]$.

[3]Following a generic assumption on PLS, i.e., the availability of the perfect channel state information (CSI) of the legitimate links and the channel distribution information of the eavesdropping links, this paper considers the optimal phase shift setting for the legitimate links only, and the beamforming design at FD DR without the perfect CSI of E [36]. In a detail, RIS cascaded channel can be estimated by utilizing the active transceivers at the transmitter and receiver (i.e., by transmitting/receiving the pilots) [37]. However, a detailed channel estimation procedure for RIS assisted communications is outside the scope of this paper.

[4]This assumption corresponds to the scenario in which there exists the several scatters if the line-of-sight (LoS) link is blocked.

[5]Such a setting corresponds to a scenario in which the DT and DR, as a single transmitter-receiver pair in the D2D networks, transmit alternatively in each transmission duration. Therefore, the sum of the powers assigned to DT and DR in the proposed setting is equal to the total power assigned to DT in the time division duplex system.

By this setting, $\widehat{\mathbf{O}}^H(\mathbf{I}_{M-1}-\mathbf{Q})=0$ can be observed, and Ω satisfy the desired condition, i.e., $\mathbf{h}_{10}^H\Omega=\mathbf{h}_{11}^H\Omega=0$. In such a way, both the SI signal at DR and the AN signal towards CR are nullified, ensuring the normal receptions at both DR and CR without the interference.

C. SIGNAL TRANSMISSION MODEL

The baseband equivalent received signals at CR, DR, and E are, respectively represented as

$$y_c=\sqrt{P_c}\left(h_1+\mathbf{h}_3^H\mathbf{\Theta}_c\mathbf{h}_2\right)x_c+\sqrt{\frac{(1-\varphi)P_d}{M-1}}\mathbf{h}_{10}^H\Omega\Upsilon+n_c, \tag{2}$$

$$y_d=\sqrt{\varphi P_d}\left(\mathbf{h}_7^H\mathbf{\Theta}_d\mathbf{h}_6\right)x_d+\sqrt{\frac{(1-\varphi)P_d}{M-1}}\mathbf{h}_{11}^H\Omega\Upsilon+n_d, \tag{3}$$

and

$$y_e=\sqrt{P_c}\left(h_4+\mathbf{h}_5^H\mathbf{\Theta}_c\mathbf{h}_2\right)x_c+\sqrt{\varphi P_d}\left(\mathbf{h}_8^H\mathbf{\Theta}_d\mathbf{h}_6\right)x_d+\sqrt{\frac{(1-\varphi)P_d}{M-1}}\mathbf{h}_9^H\Omega\Upsilon+n_e, \tag{4}$$

where $\mathbf{\Theta}_c=\text{diag}\{\beta_c^1e^{j\phi_c^1},\ldots,\beta_c^Re^{j\phi_c^R}\}\in\mathbb{C}^{R\times R}$, and $\mathbf{\Theta}_d=\text{diag}\{\beta_d^1e^{j\phi_d^1},\ldots,\beta_d^Se^{j\phi_d^S}\}\in\mathbb{C}^{S\times S}$ are the phase-shift matrices of RiS_c and RiS_d, respectively. In a detail, $\phi_c^r(\phi_d^s)\in[0,2\pi)$, and $\beta_c^r(\beta_d^s)\in[0,1]$, $\forall r=1,\ldots,R\,(s=1,\ldots,S)$ are the phase shift and reflection amplitude induced by the $r^{th}(s^{th})$ reflecting element in RiS_c (RiS_d), respectively. The simplified model of the reflection amplitudes, i.e., $\beta_c^r=\beta_d^s=1$, is used for maximization of the reflected power of the intended signal and thus the reduction of the hardware cost [38], [39]. Furthermore, x_c, $\mathbb{E}\left\{|x_c|^2\right\}=1$, and x_d, $\mathbb{E}\left\{|x_d|^2\right\}=1$, are the Gaussian modulated signals intended for CR and DR, respectively. n_c, n_d, and n_e, with the variance σ_c^2, σ_d^2, and σ_e^2, denote the additive white Gaussian noise (AWGN) related to the receiving antenna of CR, DR, and E, respectively. The independent, identically distributed noise, i.e., $\sigma^2=\sigma_c^2=\sigma_d^2=\sigma_e^2$, is considered for the mathematical tractability. In this respect, $\rho_c\triangleq\frac{P_c}{\sigma^2}$, $\rho_d\triangleq\frac{\varphi P_d}{\sigma^2}$, and $\rho_j\triangleq\frac{(1-\varphi)P_d}{(M-1)\sigma^2}$ are the SNR at CT, DT, and DR, respectively [40]. Furthermore, P_c is the power assigned to the cellular network. By nullifying the AN signals in the directions of CR and DR,[6] the SINRs decoding x_c and x_d at CR and DR are simplified as

$$\gamma_L^C=\rho_c|h_1+\mathbf{h}_3^H\mathbf{\Theta}_c\mathbf{h}_2|^2, \tag{5}$$

and

$$\gamma_L^D=\rho_d|\mathbf{h}_7^H\mathbf{\Theta}_d\mathbf{h}_6|^2, \tag{6}$$

respectively.

Similarly, the SINRs decoding x_c and x_d at E are denoted by

$$\gamma_E^C=\frac{\rho_c|h_4+\mathbf{h}_5^H\mathbf{\Theta}_c\mathbf{h}_2|^2}{\rho_d|\mathbf{h}_8^H\mathbf{\Theta}_d\mathbf{h}_6|^2+\rho_j\|\mathbf{h}_9^H\Omega\|^2+1}, \tag{7}$$

and

$$\gamma_E^D=\frac{\rho_d|\mathbf{h}_8^H\mathbf{\Theta}_d\mathbf{h}_6|^2}{\rho_c|h_4+\mathbf{h}_5^H\mathbf{\Theta}_c\mathbf{h}_2|^2+\rho_j\|\mathbf{h}_9^H\Omega\|^2+1}, \tag{8}$$

respectively.

III. STATISTICAL CHARACTERIZATION OF RIS-ASSISTED E2E WIRELESS CHANNELS

This section presents the theoretical framework of the statistical characterization of the RIS-assisted E2E legitimate and eavesdropping wireless channels in the cellular and D2D networks.

A. E2E LEGITIMATE CHANNEL IN CELLULAR NETWORK

Based on the available CSI, RiS_c adjusts the phase shifts as $\phi_c^r=\arg(h_1)-\arg([\mathbf{h}_3]_r[\mathbf{h}_2]_r)$ to maximize the intended SINR (i.e., γ_L^C). As a result, $h_1+\mathbf{h}_3^H\mathbf{\Theta}_c\mathbf{h}_2$ is revised as $h_1+\sum_{r=1}^R|[\mathbf{h}_3]_r[\mathbf{h}_2]_r|$. Let $\mathbf{h}_{3,2}=\mathbf{h}_3\odot\mathbf{h}_2$, where $[\mathbf{h}_{3,2}]_r$ represents the channel amplitude of x_c incident on the r^{th} reflecting element of RiS_c, and then reflected towards CR, and is subject to the double-Rayleigh fading. The following Lemma shows the statistical properties of $[\mathbf{h}_{3,2}]_r$.

Lemma 1: The mean and variance of $[\mathbf{h}_{3,2}]_r$ *are given by* $\mathbb{E}\left\{|[\mathbf{h}_{3,2}]_r|\right\}=\frac{\pi}{4}$ *and* $\mathbb{V}\left\{|[\mathbf{h}_{3,2}]_r|\right\}=\frac{16-\pi^2}{16}$, *respectively.*

Proof: See Appendix A. □

Furthermore, $\mathbf{h}_{3,2}=\sum_{r=1}^R[\mathbf{h}_{3,2}]_r$ is the sum of R i.i.d. double Rayleigh $\mathcal{RV}$s, and using the central limit theorem (CLT) for a sufficiently large R, is approximated by the Gaussian distributed $\mathcal{RV}$ with mean $\mathbb{E}\left\{|\mathbf{h}_{3,2}|\right\}=\frac{R\pi}{4}$ and variance $\mathbb{V}\left\{|\mathbf{h}_{3,2}|\right\}=\frac{R(16-\pi^2)}{16}$ [42]. The effective channel power for CR is defined as $\Lambda_c=\left(|h_1|+|\mathbf{h}_{3,2}|\right)^2$, which is the square of the sum of the Rayleigh and Gaussian distributed $\mathcal{RV}$s. By using the moment matching technique for the distribution approximations [43], Λ_c is approximated with a regular gamma distribution, i.e., $\Lambda_c\dot{\sim}\Gamma(k_c,\theta_c)$. The shape parameter k_c, and scale parameter θ_c, are given by

$$k_c=\frac{\mathbb{E}\{\Lambda_c\}^2}{\mathbb{E}\left\{\Lambda_c^2\right\}-\mathbb{E}\{\Lambda_c\}^2}, \tag{9}$$

and

$$\theta_c=\frac{\mathbb{E}\left\{\Lambda_c^2\right\}-\mathbb{E}\{\Lambda_c\}^2}{\mathbb{E}\{\Lambda_c\}}, \tag{10}$$

[6] In practice, the antenna m at DR receives the jamming signal, Υ, due to the FD operation, and the jamming signal must be canceled for a reliable reception of x_d [41]. The signal received at DR can be written as $\sqrt{\varphi P_d}\left(\mathbf{h}_7^H\Theta_\mathbf{d}\mathbf{h}_6\right)x_d+\sqrt{b_{sic}\times\frac{(1-\varphi)P_d}{M-1}}\mathbf{h}_{11}^H\Omega\Upsilon+n_d$, where $\sqrt{b_{sic}\times\frac{(1-\varphi)P_d}{M-1}}\mathbf{h}_{11}^H\Omega\Upsilon$ indicates the residual SI after the beamforming procedure. $0\le b_{sic}\le1$ is the SI elimination factor (i.e., $b_{sic}=0$ indicates the nullified SI, and $b_{sic}=1$ is the maximum SI or invalid beamforming). Importantly, the perfect estimation of $\mathbf{h}_{11}$ is required to nullify the SI and is not possible in the practical systems. However, because beamforming is implemented to nullify the AN in the directions of DR and CR, the residual SI at DR is very small (as compared to the AN signal that deteriorate the channel of E), and thus can be ignored, i.e., $b_{sic}=0$.

respectively, where $\mathbb{E}\{\Lambda_c\}$ and $\mathbb{E}\left\{\Lambda_c^2\right\}$ are the first and second moments of Λ_c, respectively.

The following theorem determines the parameters k_c and θ_c.

Theorem 1: The parameters, k_c and θ_c, are expressed by

$$\mathbb{E}\{\Lambda_c\} = 1 + \frac{R\left(16-\pi^2\right)}{16} + \left(\frac{R\pi}{4}\right)^2 + \frac{R\pi\sqrt{\pi}}{4}, \tag{11}$$

and

$$\begin{aligned}\mathbb{E}\left\{\Lambda_c^2\right\} = &\left(\frac{R\pi}{4}\right)^4 + 6\left(\frac{R\pi}{4}\right)^2\left(\frac{R\left(16-\pi^2\right)}{16}\right)\\ &+3\left(\frac{R\left(16-\pi^2\right)}{16}\right)^2\\ &+2\sqrt{\pi}\left(\left(\frac{R\pi}{4}\right)^3 + 3\left(\frac{R\left(16-\pi^2\right)}{16}\right)\left(\frac{R\pi}{4}\right)\right)\\ &+6\left(\frac{R\left(16-\pi^2\right)}{16} + \left(\frac{R\pi}{4}\right)^2\right) + 3R\pi\sqrt{\pi} + 2\end{aligned} \tag{12}$$

respectively. Substituting Eqs. (11) and (12) into Eqs. (9) and (10), the parameters k_c and θ_c are respectively obtained.

Proof: See Appendix B. □

B. E2E LEGITIMATE CHANNEL IN D2D NETWORK

Following a similar approach for the D2D network, RiS_d adjusts the phase shifts as $\phi_d^s = \phi_{7s} + \phi_{6s}$ to maximize the intended SINR (i.e., γ_L^D), where ϕ_{7s} and ϕ_{6s} are the phases of $[\mathbf{h}_7]_s$ and $[\mathbf{h}_6]_s$, respectively. Consequently, $\mathbf{h}_7^H\boldsymbol{\Theta}_d\mathbf{h}_6$ is revised as $\sum_{s=1}^{S}|[\mathbf{h}_7]_s[\mathbf{h}_6]_s|$. Let $\mathbf{h}_{7,6} = \mathbf{h}_7 \odot \mathbf{h}_6$, where $[\mathbf{h}_{7,6}]_s$ represents the channel amplitude of x_d incident on the s^{th} reflecting element of RiS_d, and then reflected towards the DR, and is subject to the double-Rayleigh fading with the statistical properties easily determined using Lemma 1. Using CLT for a sufficiently large S, $\mathbf{h}_{7,6} = \sum_{s=1}^{S}[\mathbf{h}_{7,6}]_s$ is approximated with a Gaussian distributed $\mathcal{RV}$ with mean $\mathbb{E}\left\{|\mathbf{h}_{7,6}|\right\} = \frac{S\pi}{4}$ and variance $\mathbb{V}\left\{|\mathbf{h}_{7,6}|\right\} = \frac{S(16-\pi^2)}{16}$. The channel power for the DR in the D2D network, $\Lambda_d = |\mathbf{h}_{7,6}|^2$, is the square of Gaussian $\mathcal{RV}$ only, and can also be approximated with a regular gamma distribution, i.e., $\Lambda_d \dot{\sim} \Gamma(k_d, \theta_d)$, using the moment matching technique [44]. Following the similar steps, the shape and scale parameters of Λ_d, i.e., k_d and θ_d, can be derived using the first and second moments as

$$\mathbb{E}\{\Lambda_d\} = \left(\frac{S\pi}{4}\right)^2 + \frac{S\left(16-\pi^2\right)}{16}, \tag{13}$$

and

$$\begin{aligned}\mathbb{E}\left\{\Lambda_d^2\right\} = &\left(\frac{S\pi}{4}\right)^4 + 6\left(\frac{S\pi}{4}\right)^2\left(\frac{S\left(16-\pi^2\right)}{16}\right)\\ &+3\left(\frac{S\left(16-\pi^2\right)}{16}\right)^2.\end{aligned} \tag{14}$$

C. E2E EAVESDROPPING CHANNELS

Without the perfect CSI, RiS_c and RiS_d cannot adjust the phase shifts of their respective reflecting elements according to the fading gain phases of the eavesdropping links, and therefore the optimal setting of phase shifts is not obtained [45]. Consequently, the eavesdropping SINRs, γ_E^C and γ_E^D can be rewritten as

$$\gamma_E^C = \frac{\rho_c t_1}{\rho_d t_2 + \rho_j t_3 + 1}, \tag{15}$$

and

$$\gamma_E^D = \frac{\rho_d t_2}{\rho_c t_1 + \rho_j t_3 + 1}, \tag{16}$$

respectively. Here,

$$t_1 = \left|\,|[h_4]_r|\,e^{-j\phi_{4r}} + \sum_{r=1}^{R} e^{j\left(\phi_c^r - \phi^{2r} - \phi^{5r}\right)}|[\mathbf{h}_2]_r[\mathbf{h}_5]_r|\right|^2, \tag{17}$$

$$t_2 = \left|\sum_{s=1}^{S} e^{j\left(\phi_d^s - \phi^{6s} - \phi^{8s}\right)}|[\mathbf{h}_6]_s[\mathbf{h}_8]_s|\right|^2, \tag{18}$$

and

$$t_3 = \|\mathbf{h}_9^H\Omega\|^2, \tag{19}$$

where ϕ^{2r}, ϕ^{4r}, ϕ^{5r}, ϕ^{6s}, and ϕ^{8s} are the phases of $[\mathbf{h}_2]_r$, $[\mathbf{h}_4]_r$, $[\mathbf{h}_5]_r$, $[\mathbf{h}_6]_s$, and $[\mathbf{h}_8]_s$, respectively. Furthermore, t_1 and t_2 can be approximated using the exponential $\mathcal{RV}$ with parameters $\lambda_{t_1} = R+1$ and $\lambda_{t_2} = S$, respectively. The probability density function (PDF) of t_3 also follows an exponential distribution with parameter $\lambda_{t_3} = M-1$. Here, the PDF of t_i, $i \in \{1, 2, 3\}$, is considered as $f_{t_i}(y) = \frac{1}{\lambda_{t_i}} exp^{-\frac{y}{\lambda_{t_i}}}$.

IV. ACHIEVABLE ERGODIC SECRECY RATE ANALYSIS

This section provides an analytical framework to derive the approximate achievable ergodic secrecy rates in the cellular and D2D networks.

A. ACHIEVABLE ERGODIC RATE FOR CELLULAR LEGITIMATE USER

The achievable ergodic rate associated with x_c at CR is given by

$$R_L^C = \mathbb{E}\left\{\log\left(1+\gamma_L^C\right)\right\}, \tag{20}$$

where $\gamma_L^C = \rho_c\Lambda_c$.

For $\Lambda_c \dot{\sim} \Gamma(k_c, \theta_c)$ and any scalar $\rho_c > 0$, $\rho_c\Lambda_c \dot{\sim} \Gamma(k_c, \rho_c\theta_c)$. Using Eqs. (9) and (10), we get $\rho_c\Lambda_c \dot{\sim} \Gamma\left(\frac{\mathbb{E}\{\Lambda_c\}^2}{\mathbb{E}\{\Lambda_c^2\}-\mathbb{E}\{\Lambda_c\}^2}, \rho_c\left(\frac{\mathbb{E}\{\Lambda_c^2\}-\mathbb{E}\{\Lambda_c\}^2}{\mathbb{E}\{\Lambda_c\}}\right)\right)$. Now, the following Lemma and Theorem are presented to solve Eq. (20)

Lemma 2: $\rho_c\Lambda_c \dot{\sim} \Gamma(k_c, \rho_c\theta_c)$ has the parameters k_c and $\rho_c\theta_c$, and the mean and variance of $\rho_c\Lambda_c$ are respectively given by

$$\mathbb{E}\{\rho_c\Lambda_c\} = k_c\rho_c\theta_c, \tag{21}$$

$$\mathbb{V}\{\rho_c\Lambda_c\} = k_c(\rho_c\theta_c)^2. \tag{22}$$

Proof: The proof is available in [46]. □

Theorem 2: If $\rho_c\Lambda_c$ is $\mathcal{RV}$ with mean $\mathbb{E}\{\rho_c\Lambda_c\}$ and variance $\mathbb{V}\{\rho_c\Lambda_c\}$, then $\mathbb{E}\{\ln(1+\rho_c\Lambda_c)\}$ can be approximated as

$$\mathbb{E}\{\ln(1+\rho_c\Lambda_c)\} \approx \ln(1+\mathbb{E}\{\rho_c\Lambda_c\}) - \mathbb{V}\{\rho_c\Lambda_c\}\left(\frac{1}{2(1+\mathbb{E}\{\rho_c\Lambda_c\})^2}\right), \quad (23)$$

Proof: See Appendix C. □

Using Lemma 2 and Theorem 2, as well as the algebraic manipulation, Eq. (20) can be approximated as

$$R_L^C \approx \frac{1}{\ln 2}\left\{\ln(1+k_c\rho_c\theta_c) - \frac{k_c(\rho_c\theta_c)^2}{2(1+k_c\rho_c\theta_c)^2}\right\} \quad (24)$$

Using Theorem 1 and substituting the values of k_c and θ_c obtained in Eqs. (11) and (12), Eq. (24) is solved. In this way, the approximate expression of the achievable ergodic rate at CR in cellular network is obtained.

B. ACHIEVABLE ERGODIC RATE FOR D2D LEGITIMATE USER

The achievable ergodic rate associated with symbol x_d at DR can be expressed by

$$R_L^D = \mathbb{E}\left\{\log\left(1+\gamma_L^D\right)\right\}, \quad (25)$$

where $\gamma_L^D = \rho_d\Lambda_d$.

Using the same approach, Eq. (25) can be approximated as

$$R_L^D \approx \frac{1}{\ln 2}\left\{\ln(1+k_d\rho_d\theta_d) - \frac{k_d(\rho_d\theta_d)^2}{2(1+k_d\rho_d\theta_d)^2}\right\} \quad (26)$$

By obtaining the values of k_d and θ_d using the first and second moments, i.e., $\mathbb{E}\{\Lambda_d\}$ and $\mathbb{E}\{\Lambda_d^2\}$, Eq. (26) is solved. In this way, the approximate expression of the achievable ergodic rate at DR in D2D network is obtained.

C. ACHIEVABLE ERGODIC RATE FOR EAVESDROPPER

The achievable ergodic rates associated with symbols x_c and x_d at E are given by

$$R_E^C = \mathbb{E}\left\{\log\left(1+\gamma_E^C\right)\right\}, \quad (27)$$

and

$$R_E^D = \mathbb{E}\left\{\log\left(1+\gamma_E^D\right)\right\}, \quad (28)$$

respectively.

For positive c_1, c_2, and c_3, we can rewrite $\log\left(1+\frac{c_1}{c_2+c_3}\right)$ as $\log\left(1+\frac{c_1+c_2}{c_3}\right) - \log\left(1+\frac{c_2}{c_3}\right)$. Now, Eq. (27) and (28) can be expressed as

$$R_E^C = \mathbb{E}\{\log(1+U_1)\} - \mathbb{E}\{\log(1+U_2)\}, \quad (29)$$

and

$$R_E^D = \mathbb{E}\{\log(1+U_1)\} - \mathbb{E}\{\log(1+U_3)\}, \quad (30)$$

respectively, where $U_1 = \rho_c t_1 + \rho_d t_2 + \rho_j t_3$, $U_2 = \rho_d t_2 + \rho_j t_3$, and $U_3 = \rho_c t_1 + \rho_j t_3$.

To solve Eqs. (29) and (30), the following Lemmas and Theorem are presented

Lemma 3: If $Y \dot{\sim} Exp(\kappa)$, then for the positive factor c_0, $c_0 Y \dot{\sim} Exp\left(\frac{\kappa}{c_0}\right)$.

Proof: See Appendix D. □

Lemma 4: For $1 \le k \le K$, the sum of K independent exponential $\mathcal{RV}$s with a distinct rate κ_k, (κ_k is the rate of the k^{th} exponential distribution) can be approximated by the generalized Erlang or hypoexponential distributed $\mathcal{RV}$ $U \dot{\sim} hypoexp(\kappa_1, \ldots, \kappa_k)$.

Proof: The proof is available in [47]. □

Using Lemma 3, i.e., by scaling $Y \dot{\sim} Exp(\kappa)$, the $\mathcal{RV}$s $\rho_c t_1 \dot{\sim} Exp\left(\frac{R+1}{\rho_c}\right)$, $\rho_d t_2 \dot{\sim} Exp\left(\frac{S}{\rho_d}\right)$, and $\rho_j t_3 \dot{\sim} Exp\left(\frac{M-1}{\rho_j}\right)$ are obtained. Using Lemma 4, i.e., by obtaining the distribution of the sum of K independent exponential $\mathcal{RV}$s, the statistical properties of U are determined. The mean of U, $\mathbb{E}\{U\}$, and variance of U and $\mathbb{V}\{U\}$, are $\sum_{k=1}^{K}\frac{1}{\kappa_k}$, and $\sum_{k=1}^{K}\left(\frac{1}{\kappa_k}\right)^2$, respectively. Furthermore, the following theorem solves Eqs. (29) and (30), respectively.

Theorem 3: The approximate expressions of the achievable ergodic rate associated with symbols x_c and x_d at E can be determined as

$$R_E^C \approx \frac{1}{\ln 2} \times \left\{\ln\left(\frac{1+\mathbb{E}\{U_1\}}{1+\mathbb{E}\{U_2\}}\right) - \frac{\mathbb{V}\{U_1\}}{2(1+\mathbb{E}\{U_1\})^2} + \frac{\mathbb{V}\{U_2\}}{2(1+\mathbb{E}\{U_2\})^2}\right\}, \quad (31)$$

and

$$R_E^D \approx \frac{1}{\ln 2} \times \left\{\ln\left(\frac{1+\mathbb{E}\{U_1\}}{1+\mathbb{E}\{U_3\}}\right) - \frac{\mathbb{V}\{U_1\}}{2(1+\mathbb{E}\{U_1\})^2} + \frac{\mathbb{V}\{U_3\}}{2(1+\mathbb{E}\{U_3\})^2}\right\}, \quad (32)$$

respectively, where

$$\begin{aligned}
\mathbb{E}\{U_1\} &= \frac{\rho_c}{R+1} + \frac{\rho_d}{S} + \frac{\rho_j}{M-1},\\
\mathbb{V}\{U_1\} &= \left(\frac{\rho_c}{R+1}\right)^2 + \left(\frac{\rho_d}{S}\right)^2 + \left(\frac{\rho_j}{M-1}\right)^2,\\
\mathbb{E}\{U_2\} &= \frac{\rho_d}{S} + \frac{\rho_j}{M-1},\\
\mathbb{V}\{U_2\} &= \left(\frac{\rho_d}{S}\right)^2 + \left(\frac{\rho_j}{M-1}\right)^2,\\
\mathbb{E}\{U_3\} &= \frac{\rho_c}{R+1} + \frac{\rho_j}{M-1},\\
\mathbb{V}\{U_3\} &= \left(\frac{\rho_c}{R+1}\right)^2 + \left(\frac{\rho_j}{M-1}\right)^2.
\end{aligned}$$

Proof: See Appendix E. □

D. ACHIEVABLE ERGODIC SECRECY RATE OF THE SYSTEM

Similar to [48], the achievable ergodic secrecy rate is defined as a positive discrepancy between the achievable ergodic rates for the legitimate user and eavesdropper. Using the derived expressions associated with the cellular and D2D information symbols, the achievable ergodic secrecy rates can be defined as

$$R_S^C = [R_L^C - R_E^C]^+, \tag{33}$$

and

$$R_S^D = [R_L^D - R_E^D]^+, \tag{34}$$

where $[v]^+ = max(0, v)$. R_L^C and R_E^C are calculated by Eqs. (24) and (31), and R_L^D and R_E^D are calculated by Eqs. (26) and (32), respectively.

In practice, R_S^C and R_S^D are non-negative by designing the secure transmissions for the underlay D2D networks. In this respect, the achievable ergodic secrecy rates of the system can be acquired as

$$R_S^{Total} = R_S^C + R_S^D. \tag{35}$$

V. NUMERICAL RESULTS

This section presents the numerical results to verify the analytical results presented in the previous sections, and provides the valuable insights. If not specified otherwise, the main parameters are set as $R = 60$, $S = 30$, $M = 15$, and $\frac{P_c}{\sigma^2} = \frac{P_d}{\sigma^2} = 10$dB, and are selected for a behavioral validation of the system. For the comparison, the benchmark scheme in [32] is plotted in which the jamming signals for the cellular network were provided via a D2D RIS-cascaded channel, and only a direct link (i.e., without a RIS-cascaded channel) was used for a cellular user. Moreover, D2D users in [32] were evaluated in terms of the reliability performance only. In order to evaluate the performance of the cellular network comprehensively, the baseline scheme is also plotted in which the cellular networks used only a RIS-cascaded channel (i.e., without a direct link), and were not provided the jamming signals (i.e., no cooperation between the networks). The simulation results are obtained via the Monte Carlo simulations with 10^7 channel realizations. Notably, the numerical and simulation results are consistent and therefore verify the accuracy of the presented analytical framework.

A. PERFORMANCE OF THE CELLULAR NETWORKS

First, the performance of the cellular networks is evaluated in terms of the achievable ergodic secrecy rates. Fig. 2 shows the relationship between the achievable ergodic rates at CR, R_L^C, with the SNR at CT, ρ_c. The analysis point is calculated by Eq. (24). The results show that R_L^C exhibits an incremental relationship with ρ_c, and the presented framework provides a superior performance compared to the benchmark and baseline schemes. This is because the presented framework considers both direct and RIS-cascaded links. R_L^C can be enhanced by the RIS, instead of increasing ρ_c or a relay link, for the SINR improvement. This is justified by the degree

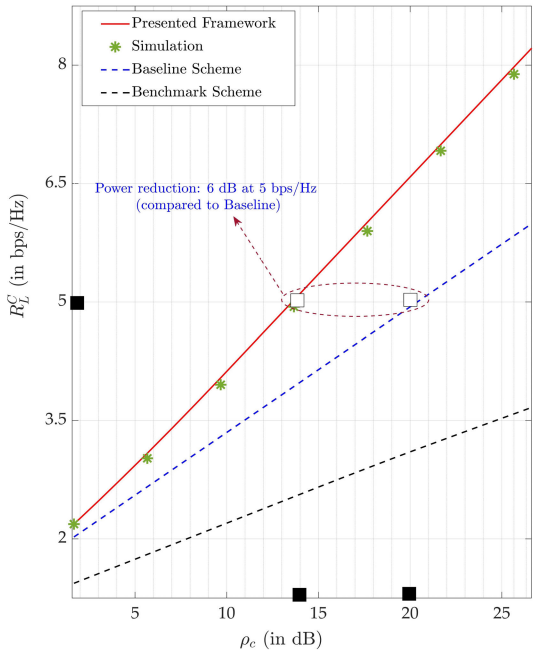

FIGURE 2. Achievable ergodic rates at CR vs. SNR at CT (ρ_c).

of freedom achieved by the optimal phase shifting and the amount of additional information that can be transmitted using the proposed framework. In contrast, the benchmark scheme provides the worst performance because it is based on an environment where RIS does not exist.

Fig. 3 depicts the relationship between the achievable ergodic rates at E, R_E^C, with ρ_c, and provides a performance comparison with the benchmark and baseline schemes. The analysis point is calculated by Eq. (31). In the presented framework, the jamming signals for the cellular network are provided from both the DT (via RIS-cascaded channel), and multi-antenna DR. In contrast, only the single-antenna DT provides the jamming signals in benchmark strategy. As expected, R_E^C also increases with ρ_c, due to the increase in leakage information. The presented framework guarantees a superior performance in comparison to baseline scheme for which there is no cooperation from D2D network in terms of jamming signals. The superior performance of the presented framework in comparison to benchmark scheme relies on the D2D power allocation strategy.

Fig. 4 plots the achievable ergodic secrecy rates in the cellular network, R_S^C and ρ_c, and presents a performance comparison with the benchmark and baseline schemes. The analysis point is calculated by Eq. (33). For all the schemes, R_S^C first increases and then decreases as ρ_c increases, demonstrating that ρ_c can be optimized. This implies a trade-off between the security and reliability in the event of an eavesdropping attack, referred as the security-reliability trade-off. The presented framework provides best performance in terms of R_S^C by utilizing the proper D2D power allocation strategy. By adjusting the D2D power allocations, the achievable ergodic rates associated with x_c at CR exceed than that at E, and therefore higher R_S^C points are attainable throughout

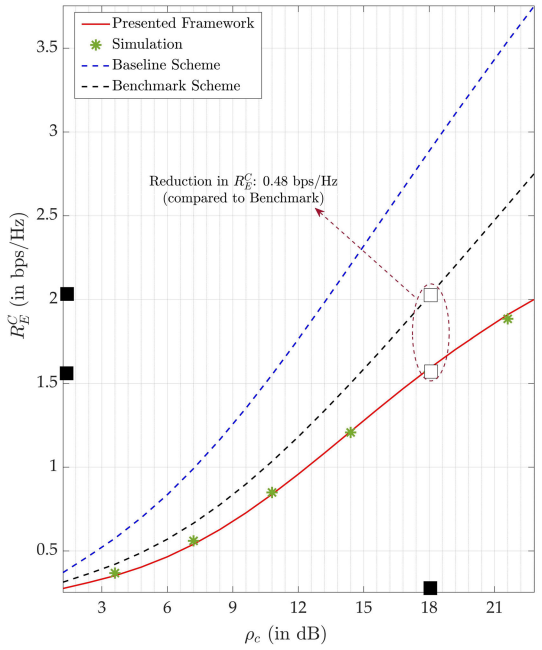

FIGURE 3. Achievable ergodic rates at E vs. SNR at CT (ρ_c).

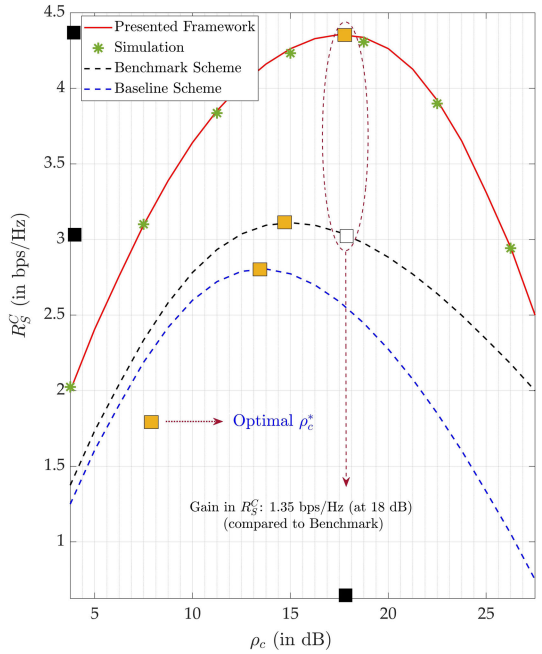

FIGURE 4. Achievable ergodic secrecy rates of the cellular network vs. SNR at CT (ρ_c).

ρ_c. The benchmark outperforms the baseline scheme as it provides a comparatively lesser leakage information due to the jamming signals.

B. PERFORMANCE OF THE OVERALL SYSTEM

Now, the achievable ergodic secrecy rate performance of the overall system is evaluated. Fig. 5 shows the relationship between the total achievable ergodic rates at the legitimate users, CR and DR, i.e., $R_L^C + R_L^D$, with D2D power allocation ratio (φ). The analysis points are calculated by

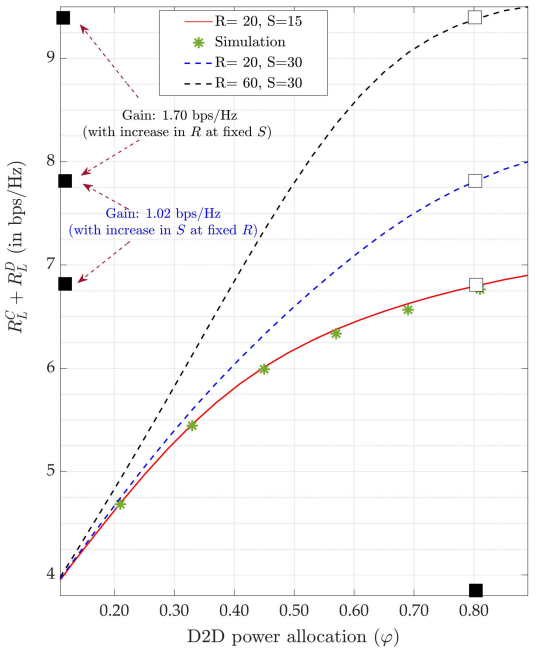

FIGURE 5. Total achievable ergodic rates at CR and DR vs. D2D power allocation ratio (φ).

Eqs. (24) and (26). Here, the relationship is also incremental. Importantly, the presented framework provides the maximum decoding SINRs at CR, given by Eq. (5), and DR, given by Eq. (6), and thus provides an optimal performance in terms of total achievable ergodic rates. This is justified by the argument that the AN signals in the direction of the CR and DR are eliminated by adapting the proposed beamforming design; therefore, the interference is minimized. It can also be observed that the reflecting elements in both networks, i.e., R and S, have a positive impact on the performance. By an optimal phase shift setting, increase in reflecting elements enables an efficient exploitation of the spatial degrees of freedom, providing substantial performance gain.

Fig. 6 depicts the relationship between the total achievable ergodic rates at E, i.e., $R_E^C + R_E^D$, with φ. The analysis points are calculated by Eqs. (31) and (32). In the presented framework, the total SINR decoding x_c and x_d at E increase with an increment in φ, and consequently, φ is directly proportional to the total achievable ergodic rates at E. It is observed that the information leakage also increases with a increase in both R and S. It verifies that E manages to receive R and S number of copies of the intended signals, although RiS_c and RiS_d do not optimally adjust the phases for their eavesdropping links (due to absence of CSI), and cannot maximize γ_E^C and γ_E^D, respectively.

Fig. 7 plots the achievable ergodic secrecy rates of the system, R_S^{Total} with φ, R, and S. While validating the previous results in Fig. 5 and Fig. 6, the results show an increment in R_S^{Total} first, and then a decrement, as φ increases, and demonstrate that for a given number of R and S, there exists an optimal φ (φ^*) to maximize R_S^{Total}. Another important

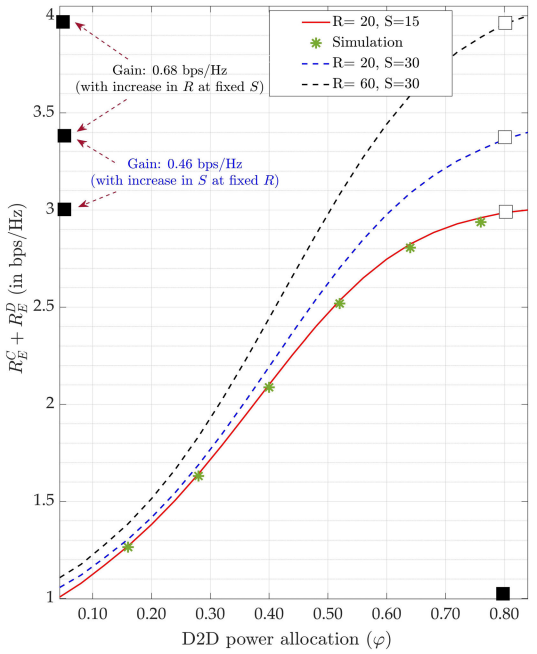

FIGURE 6. Total achievable ergodic rates at E vs. D2D power allocation ratio (φ).

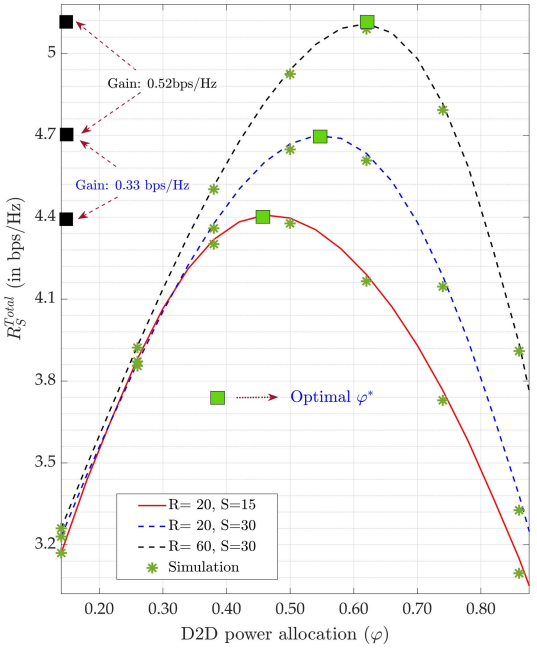

FIGURE 7. Achievable ergodic secrecy rates of the system vs. D2D power allocation ratio (φ).

observation is that the positive impact of R and S in terms of R_S^{Total} is attainable although the increase in R and S increases the total achievable ergodic rates both at the legitimate users and E.

Fig. 8 illustrates φ^* for different number of reflecting elements in RiS_c, and RiS_d. The analytical solution, i.e., φ^* for the maximum R_S^{Total}, is obtained for different number of

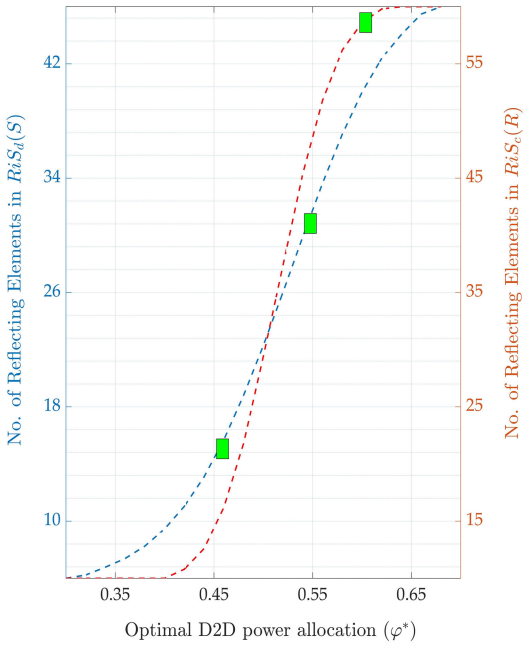

FIGURE 8. Reflecting elements vs. optimal D2D power allocation ratio (φ^*).

R and S. It is observed that φ^* has an incremental relationship for both R and S. Our results identify the optimal selection of D2D power allocations according to the number of reflecting elements in D2D and cellular networks, and provide guidelines for the robustness and security enhancements of the RIS-assisted underlay D2D networks.

VI. CONCLUSION

Despite the potential of the key technologies, 5G networks will not meet all the requirements of a post-2030 world, which necessitates the designing of 6G networks. The anticipated approaches for 6G networks include the RIS, efficient spectrum sharing, FD communication, massive MIMO, and PLS. This paper presented a novel analytical framework of spectrum sharing for the underlay D2D networks to enhance the robustness and security of the system under an eavesdropping attempt, using a combination of the RIS technology and FD jamming receiver. We statistically characterized the E2E channel powers and derived the approximate expressions for the achievable ergodic secrecy rates. The derived analytical expressions provided an easy selection of the optimal D2D power allocations for different number of reflecting elements. The results could provide design insights into the architecture of the RIS-assisted underlay D2D networks to be implemented in the 6G era.

APPENDIX A
PROOF OF LEMMA 1

Given $|[\mathbf{h}_3]_r|$ and $|[\mathbf{h}_2]_r|$ following the Rayleigh distributions, $[\mathbf{h}_{3,2}]_r$ is subject to a double-Rayleigh fading. Therefore, the closed-form PDF of $[\mathbf{h}_{3,2}]_r$ can be

determined by,

$$f_{[\mathbf{h}_{3,2}]_r}(y) = \int_0^\infty \frac{1}{x} f_{|[\mathbf{h}_3]_r|}\left(\frac{y}{x}\right) f_{|[\mathbf{h}_2]_r|}(x)\, dx = 4yK_0(2y). \quad (36)$$

Moreover, the mean and variance of $[\mathbf{h}_{3,2}]_r$ can be calculated as,

$$\mathbb{E}\left\{|[\mathbf{h}_{3,2}]_r|\right\} = \int_0^\infty 4y^2 K_0(2y)\, dy = \frac{\pi}{4}, \quad (37)$$

and

$$\mathbb{V}\left\{|[\mathbf{h}_{3,2}]_r|\right\} = \int_0^\infty 4y^3 K_0(2y)\, dy - \frac{\pi^2}{16} = \frac{16-\pi^2}{16}, \quad (38)$$

respectively. This proves the proposition.

APPENDIX B
PROOF OF THEOREM 1

Using the moment matching technique, the first moment of Λ_c, $\mathbb{E}\{\Lambda_c\}$, is determined as,

$$\mathbb{E}\{\Lambda_c\} = \mathbb{E}\left\{\left(|h_1| + |\mathbf{h}_{3,2}|\right)^2\right\} = \mathbb{E}\left\{|h_1|^2\right\} + \mathbb{E}\left\{|\mathbf{h}_{3,2}|^2\right\} + 2\mathbb{E}\{|h_1|\}\,\mathbb{E}\left\{|\mathbf{h}_{3,2}|\right\}. \quad (39)$$

By substituting the statistics associated with a Rayleigh distributed h_1, and a Gaussian distributed $\mathbf{h}_{3,2}$, i.e.,

$$\mathbb{E}\{|h_1|\} = \frac{\sqrt{\pi}}{2},$$
$$\mathbb{E}\left\{|h_1|^2\right\} = \mathbb{V}\{|h_1|\} + (\mathbb{E}\{|h_1|\})^2 = \frac{4-\pi}{4} + \frac{\pi}{4} = 1,$$
$$\mathbb{E}\left\{|\mathbf{h}_{3,2}|\right\} = \frac{R\pi}{4},$$

and

$$\mathbb{E}\left\{|\mathbf{h}_{3,2}|^2\right\} = \mathbb{V}\left\{|\mathbf{h}_{3,2}|\right\} + \left(\mathbb{E}\left\{|\mathbf{h}_{3,2}|\right\}\right)^2 = \frac{R(16-\pi^2)}{16} + \left(\frac{R\pi}{4}\right)^2,$$

in Eq. (39), the first moment of Λ_c is obtained.

Similarly, the second moment of Λ_c, $\mathbb{E}\left\{\Lambda_c^2\right\}$, is determined by,

$$\mathbb{E}\left\{\Lambda_c^2\right\} = \mathbb{E}\left\{\left(|h_1| + |\mathbf{h}_{3,2}|\right)^4\right\} = \mathbb{E}\left\{|\mathbf{h}_{3,2}|^4\right\} + \binom{4}{1}\mathbb{E}\{|h_1|\}\,\mathbb{E}\left\{|\mathbf{h}_{3,2}|^3\right\} + \binom{4}{2}\mathbb{E}\left\{|h_1|^2\right\}\mathbb{E}\left\{|\mathbf{h}_{3,2}|^2\right\} + \binom{4}{3}\mathbb{E}\left\{|h_1|^3\right\}\mathbb{E}\left\{|\mathbf{h}_{3,2}|\right\} + \mathbb{E}\left\{|h_1|^4\right\}. \quad (40)$$

Following the similar procedure and substituting the statistics, i.e.,

$$\mathbb{E}\left\{|\mathbf{h}_{3,2}|^4\right\} = \left(\mathbb{E}\left\{|\mathbf{h}_{3,2}|\right\}\right)^4 + 6\left(\mathbb{E}\left\{|\mathbf{h}_{3,2}|\right\}\right)^2 \mathbb{V}\left\{|\mathbf{h}_{3,2}|\right\} + 3\left(\mathbb{V}\left\{|\mathbf{h}_{3,2}|\right\}\right)^2 = \left(\frac{R\pi}{4}\right)^4 + 6\left(\frac{R\pi}{4}\right)^2\left(\frac{R(16-\pi^2)}{16}\right) + 3\left(\frac{R(16-\pi^2)}{16}\right)^2,$$
$$\mathbb{E}\left\{|\mathbf{h}_{3,2}|^3\right\} = \left(\mathbb{E}\left\{|\mathbf{h}_{3,2}|\right\}\right)^3 + 3\mathbb{E}\left\{|\mathbf{h}_{3,2}|\right\}\mathbb{V}\left\{|\mathbf{h}_{3,2}|\right\} = \left(\frac{R\pi}{4}\right)^3 + 3\left(\frac{R\pi}{4}\right)\left(\frac{R(16-\pi^2)}{16}\right),$$
$$\mathbb{E}\left\{|h_1|^3\right\} = \frac{3\sqrt{\pi}}{4},$$

and

$$\mathbb{E}\left\{|h_1|^4\right\} = 2,$$

in Eq. (40), the second moment of Λ_c is obtained. This proves Theorem 1.

APPENDIX C
PROOF OF THEOREM 2

We use the Taylor expansions to approximate the moments of $\ln(1+\rho_c\Lambda_c)$, given the moments of $\rho_c\Lambda_c$ as finite and $\ln(1+\rho_c\Lambda_c)$ as sufficiently differentiable. By taking the Taylor series approximation for $\ln(1+\rho_c\Lambda_c)$ about the point $(\rho_c\Lambda_c)_0$, where $(\rho_c\Lambda_c)_0 \in (-1,\infty)$, we get,

$$\ln(1+\rho_c\Lambda_c) \approx \ln\left(1+(\rho_c\Lambda_c)_0\right) + \frac{\rho_c\Lambda_c - (\rho_c\Lambda_c)_0}{1+(\rho_c\Lambda_c)_0} - \frac{\left(\rho_c\Lambda_c - (\rho_c\Lambda_c)_0\right)^2}{2\left(1+(\rho_c\Lambda_c)_0\right)^2}. \quad (41)$$

By substituting $(\rho_c\Lambda_c)_0 = \mathbb{E}\{\rho_c\Lambda_c\}$ and applying $\mathbb{E}\{.\}$ to both sides of Eq. (41), Eq. (23) can be solved. This proves Theorem 2.

APPENDIX D
PROOF OF LEMMA 3

The CDF of $\mathcal{RV}$ $c_0 Y$ is given by $F_{c_0 Y}(y) = P(c_0 Y \le y) = F_Y\left(\frac{y}{c_0}\right)$, where $F_Y(.)$ is the CDF of Y. Lemma 3 proves that.

APPENDIX E
PROOF OF THEOREM 3

Using Theorem 2, algebraic manipulation, and substituting the results of Lemma 3 and 4, Eqs. (29) and (30) are solved. This concludes the proof.

REFERENCES

[1] M. A. Siddiqi, H. Yu, and J. Joung, "5G ultra-reliable low-latency communication implementation challenges and operational issues with IoT devices," *Electronics*, vol. 8, no. 9, pp. 981–999, Sep. 2019.

[2] W. Khalid, H. Yu, R. Ali, and R. Ullah, "Advanced physical-layer technologies for beyond 5G wireless communication networks," *Sensors*, vol. 21, no. 9, pp. 3197–3205, May 2020.
[3] H. Yu, H. Lee, and H. Jeon, "What is 5G? Emerging 5G mobile services and network requirements," *Sustainability*, vol. 9, no. 10, pp. 1848–1870, Oct. 2017.
[4] M. R. G. Aghdam, B. M. Tazehkand, and R. Abdolee, "On the performance analysis of mmWave MIMO-NOMA transmission scheme," *IEEE Trans. Veh. Technol.*, vol. 69, no. 10, pp. 11491–11500, Oct. 2020.
[5] R. K. Saha, "Approaches to improve millimeter-wave spectrum utilization using indoor small cells in multi-operator environments toward 6G," *IEEE Access*, vol. 8, pp. 207643–207658, Nov. 2020.
[6] W. Khalid and H. Yu, "Optimal sensing performance for cooperative and non-cooperative cognitive radio networks," *Int. J. Distrib. Sensor Netw.*, vol. 13, no. 11, pp. 1–9, Nov. 2017.
[7] W. Saad, M. Bennis, and M. Chen, "A vision of 6G wireless systems: Applications, trends, technologies, and open research problems," *IEEE Netw.*, vol. 34, no. 3, pp. 134–142, May 2020.
[8] H. Yu, M. K. Afzal, Y. B. Zikria, A. Rachedi, and F. H. P. Fitzek, "Tactile Internet: Technologies, test platforms, trials, and applications," *Future Gener. Comput. Syst.*, vol. 106, pp. 685–688, May 2020.
[9] Y. B. Zikria, H. Yu, M. K. Afzal, M. H. Rehmani, and O. Hahm, "Internet of Things (IoT): Operating system, applications and protocols design, and validation techniques," *Future Gener. Comput. Syst.*, vol. 88, pp. 699–706, Nov. 2018.
[10] B. Mao, Y. Kawamoto, and N. Kato, "AI-based joint optimization of QoS and security for 6G energy harvesting Internet of Things," *IEEE Internet Things J.*, vol. 7, no. 8, pp. 7032–7042, Aug. 2020.
[11] W. Khalid, H. Yu, and S. Noh, "Residual energy analysis in cognitive radios with energy harvesting UAV under reliability and secrecy constraints," *Sensors*, vol. 20, no. 10, pp. 2998–3017, May 2020.
[12] W. Khalid and H. Yu, "Spatial–temporal sensing and utilization in full duplex spectrum-heterogeneous cognitive radio networks for the Internet of Things," *Sensors*, vol. 19, no. 6, pp. 1441–1459, Mar. 2019.
[13] M. A. El Mossallamy, H. Zhang, L. Song, K. G. Seddik, Z. Han, and G. Y. Li, "Reconfigurable intelligent surfaces for wireless communications: Principles, challenges, and opportunities," *IEEE Trans. Cogn. Commun. Netw.*, vol. 6, no. 3, pp. 990–1002, Sep. 2020.
[14] E. Basar, M. Di Renzo, J. De Rosny, M. Debbah, M. Alouini, and R. Zhang, "Wireless communications through reconfigurable intelligent surfaces," *IEEE Access*, vol. 7, pp. 116753–116773, 2019.
[15] H. Yu and J. Joung, "Design of the power and dimension of artificial noise for secure communication systems," *IEEE Trans. Commun.*, vol. 69, no. 6, pp. 4001–4010, Jun. 2021.
[16] H. Yu, T. Kim, and H. Jafarkhani, "Wireless secure communication with beamforming and jamming in time-varying wiretap channels," *IEEE Trans. Inf. Forensics Security*, vol. 13, no. 8, pp. 2087–2100, Aug. 2018.
[17] B. Zheng, M. Wen, C. X. Wang, and X. Wang, "Secure NOMA based two-way relay networks using artificial noise and full duplex," *IEEE J. Sel. Areas Commun.*, vol. 36, no. 7, pp. 1426–1440, Jul. 2018.
[18] R. Zhang, X. Cheng, and L. Yang, "Cooperation via spectrum sharing for physical layer security in device-to-device communications underlaying cellular networks," *IEEE Trans. Wireless Commun*, vol. 15, no. 8, pp. 5651–5663, Aug. 2016.
[19] J. M. Moualeu and T. M. N. Ngatched, "Physical-layer security enhancement via relay-aided D2D communications underlaying cellular networks," *IEEE Open J. Commun. Soc.*, vol. 1, pp. 413–427, Mar. 2020.
[20] H. V. Vu and T. Le-Ngoc, "Performance analysis of underlaid full-duplex D2D cellular networks," *IEEE Access*, vol. 7, pp. 176233–176247, Dec. 2019.
[21] C. Zhang, W. Chen, C. He, and X. Li, "Throughput maximization for intelligent reflecting surface-aided device-to-device communications system," *J. Commun. Inf. Netw.*, vol. 5, no. 4, pp. 403–410, Dec. 2020.
[22] L. Li, D. Ma, H. Ren, D. Wang, X. Tang, W. Liang, and T. Bai, "Enhanced reconfigurable intelligent surface assisted mmWave communication: A federated learning approach," *China Commun.*, vol. 17, no. 10, pp. 115–128, Oct. 2020.
[23] M. Elhattab, M.-A. Arfaoui, C. Assi, and A. Ghrayeb, "Reconfigurable intelligent surface assisted coordinated multipoint in downlink NOMA networks," *IEEE Commun. Lett.*, vol. 25, no. 2, pp. 632–636, Feb. 2021.
[24] S. Bi, C. K. Ho, and R. Zhang, "Wireless powered communication: Opportunities and challenges," *IEEE Commun. Mag.*, vol. 53, no. 4, pp. 117–125, Apr. 2015.
[25] M. Wijewardena, T. Samarasinghe, K. T. Hemachandra, S. Atapattu, and J. S. Evans, "Physical layer security for intelligent reflecting surface assisted two–way communications," *IEEE Commun. Lett.*, early access, Mar. 23, 2021, doi: 10.1109/LCOMM.2021.3068102.
[26] L. Lv, Q. Wu, Z. Li, N. Al-Dhahir, and J. Chen, "Secure two-way communications via intelligent reflecting surfaces," *IEEE Commun. Lett.*, vol. 25, no. 3, pp. 744–748, Mar. 2021.
[27] J. Youn, W. Son, and B. C. Jung, "Physical-layer security improvement with reconfigurable intelligent surfaces for 6G wireless communication systems," *Sensors*, vol. 21, no. 4, p. 1439, Feb. 2021.
[28] Y. Zhang, Y. Shen, X. Jiang, and S. Kasahara, "Mode selection and spectrum partition for D2D inband communications: A physical layer security perspective," *IEEE Trans. Commun.*, vol. 67, no. 1, pp. 623–638, Jan. 2019.
[29] M. K. Shukla, H. H. Nguyen, and O. J. Pandey, "Secrecy performance analysis of two-way relay non-orthogonal multiple access systems," *IEEE Access*, vol. 8, pp. 39502–39512, Mar. 2020.
[30] K. Cao, B. Wang, H. Ding, L. Lv, R. Dong, T. Cheng, and F. Gong, "Improving physical layer security of uplink NOMA via energy harvesting jammers," *IEEE Trans. Inf. Forensics Security*, vol. 16, pp. 786–799, Sep. 2021.
[31] Z. Kong, S. Yang, D. Wang, and L. Hanzo, "Robust beamforming and jamming for enhancing the physical layer security of full duplex radios," *IEEE Trans. Inf. Forensics Security*, vol. 14, no. 12, pp. 3151–3159, Dec. 2019.
[32] M. H. Khoshafa, T. M. N. Ngatched, and M. H. Ahmed, "Reconfigurable intelligent surfaces-aided physical layer security enhancement in D2D underlay communications," *IEEE Commun. Lett.*, vol. 25, no. 5, pp. 1443–1447, May 2021.
[33] M. H. Khoshafa, T. M. N. Ngatched, M. H. Ahmed, and A. Ibrahim, "Improving physical layer security of cellular networks using full-duplex jamming relay-aided D2D communications," *IEEE Access*, vol. 8, pp. 53575–53586, Mar. 2020.
[34] M. H. Khoshafa, T. M. N. Ngatched, M. H. Ahmed, and A. Ibrahim, "Secure transmission in wiretap channels using full-duplex relay-aided D2D communications with outdated CSI," *IEEE Wireless Commun. Lett.*, vol. 9, no. 8, pp. 1216–1220, Aug. 2020.
[35] Q. Wu and R. Zhang, "Towards smart and reconfigurable environment: Intelligent reflecting surface aided wireless network," *IEEE Commun. Mag.*, vol. 58, no. 1, pp. 106–112, Jan. 2020.
[36] W. Khalid and H. Yu, "Security improvement with QoS provisioning using service priority and power allocation for NOMA-IoT networks," *IEEE Access*, vol. 9, pp. 9937–9948, Jan. 2021.
[37] C. Hu, L. Dai, S. Han, and X. Wang, "Two-timescale channel estimation for reconfigurable intelligent surface aided wireless communications," *IEEE Trans. Commun.*, early access, Apr. 12, 2021, doi: 10.1109/TCOMM.2021.3072729.
[38] A. Hemanth, K. Umamaheswari, A. C. Pogaku, D.-T. Do, and B. M. Lee, "Outage performance analysis of reconfigurable intelligent surfaces-aided NOMA under presence of hardware impairment," *IEEE Access*, vol. 8, pp. 212156–212165, Nov. 2020.
[39] A.-A.-A. Boulogeorgos and A. Alexiou, "Performance analysis of reconfigurable intelligent surface-assisted wireless systems and comparison with relaying," *IEEE Access*, vol. 8, pp. 94463–94483, May 2020.
[40] W. Khalid and H. Yu, "Sum Utilization of spectrum with spectrum handoff and imperfect sensing in interweave multi-channel cognitive radio networks," *Sustainability*, vol. 10, no. 6, pp. 1764–1782, May 2018.
[41] H.-M. Wang, B.-Q. Zhao, and T.-X. Zheng, "Adaptive full-duplex jamming receiver for secure D2D links in random networks," *IEEE Trans. Commun.*, vol. 67, no. 2, pp. 1254–1267, Feb. 2019.
[42] Z. Ding, R. Schober, and H. V. Poor, "On the impact of phase shifting designs on IRS-NOMA," *IEEE Wireless Commun. Lett.*, vol. 9, no. 10, pp. 1596–1600, Oct. 2020.
[43] S. Atapattu, C. Tellambura, and H. Jiang, "A mixture gamma distribution to model the SNR of wireless channels," *IEEE Trans. Wireless Commun.*, vol. 10, no. 12, pp. 4193–4203, Dec. 2011.
[44] S. Atapattu, R. Fan, P. Dharmawansa, G. Wang, J. Evans, and T. A. Tsiftsis, "Reconfigurable intelligent surface assisted two-way communications: Performance analysis and optimization," *IEEE Trans. Commun.*, vol. 68, no. 10, pp. 6552–6567, Oct. 2020.
[45] L. Yang, J. Yang, W. Xie, M. O. Hasna, T. Tsiftsis, and M. D. Renzo, "Secrecy performance analysis of RIS-aided wireless communication systems," *IEEE Trans. Veh. Technol*, vol. 69, no. 10, pp. 12296–12300, Oct. 2020.

[46] F. Govaers and H. Alqaderi, "A gamma filter for positive parameter estimation," in *Proc. IEEE Int. Conf. Multisensor Fusion Integr. Intell. Syst. (MFI)*, Karlsruhe, Germany, Sep. 2020, pp. 40–45.
[47] G. P. Yanev, "Exponential and hypoexponential distributions: Some characterizations," *Mathematics*, vol. 8, no. 12, pp. 2207–2217, Dec. 2020.
[48] H. Yu and I.-G. Lee, "Physical layer security based on NOMA and AJ for MISOSE channels with an untrusted relay," *Future Gener. Comput. Syst.*, vol. 102, pp. 611–618, Jan. 2020.

WAQAS KHALID received the B.S. degree in electronics engineering from the GIK Institute of Engineering Sciences and Technology, KPK, Pakistan, in 2011, and the M.S. and Ph.D. degrees in information and communication engineering from Inha University, Incheon, South Korea, and Yeungnam University, Gyeongsan, South Korea, in 2016 and 2019, respectively. He is currently working as a Research Professor with the Institute of Industrial Technology, Korea University, Sejong, South Korea. His research interests include physical layer modeling, signal processing for wireless communications, and emerging solutions and technologies for 5G/B5G networks, such as reconfigurable intelligent surfaces, energy harvesting, physical layer security, NOMA, cognitive radio, UAVs, and the IoTs. He served as a Lead Guest Editor for Sensors Special Issue on "Advanced Physical-Layer Technologies for beyond 5G Wireless Communication Networks," in 2020. He is also serving as a Lead Guest Editor for Sensors Special Issue on "Future of Physical Layer Technologies for 6G Wireless Communication Networks."

HEEJUNG YU (Senior Member, IEEE) received the B.S. degree in radio science and engineering from Korea University, Seoul, South Korea, in 1999, and the M.S. and Ph.D. degrees in electrical engineering from the Korea Advanced Institute of Science and Technology, Daejeon, South Korea, in 2001 and 2011, respectively. From 2001 to 2012, he was with the Electronics and Telecommunications Research Institute, Daejeon, South Korea, and Yeungman University, Gyeongsan, South Korea, from 2012 to 2019. He is currently an Associate Professor with the Department of Electronics and Information Engineering, Korea University, Sejong, South Korea. His research interests include statistical signal processing and communication theory.

DINH-THUAN DO (Senior Member, IEEE) received the B.S., M.Eng., and Ph.D. degrees in communications engineering from Viet Nam National University (VNU-HCM), in 2003, 2007, and 2013, respectively. He is currently an Assistant Professor with the Department of Computer Science and Information Engineering, College of Information and Electrical Engineering, Asia University, Taichung, Taiwan. His publications include over 95 SCIE-indexed journal articles, one textbook, and five book chapters. His research interests include signal processing in wireless communications networks, NOMA, cognitive radio, physical layer security, reconfigurable intelligent surfaces aided systems, satellite systems, full-duplex transmission, and energy harvesting. He was a recipient of the Golden Globe Award from the Vietnam Ministry of Science and Technology, in 2015 (top ten most excellent scientist nationwide). He is also serving as an Associate Editor for top journals, including the *EURASIP Journal on Wireless Communications and Networking*, *Computer Communications* (Elsevier), and *KSII Transactions on Internet and Information Systems*.

ZEESHAN KALEEM (Senior Member, IEEE) received the B.S. degree in electronics engineering from the University of Engineering and Technology (UET), Peshawar, in 2007, the M.S. degree in electronics engineering from Hanyang University, South Korea, in 2010, and the Ph.D. degree in electronics engineering from Inha University, South Korea, in 2016. He is currently an Assistant Professor with the Department of Electrical and Computer Engineering, COMSATS University Islamabad, Wah Campus, Pakistan. He has published over 60 technical journal articles, book chapters, and conference papers in reputable journals/venues, and has 21 U.S. and Korean registered patents. His current research interests include public safety networks, 5G system testing and development, and unmanned air vehicle (UAV) communications. He consecutively received the National Research Productivity Award (RPA) from the Pakistan Council of Science and Technology (PSCT), for the period 2016–2018. He won the only Higher Education Commission (HEC) Best Innovator Award, for the year 2017. He was a co-recipient of the Best Research Proposal Award from SK Telecom, South Korea. He is serving as an Associate Technical Editor for prestigious journals/magazines, like *IEEE Communications Magazine*, IEEE Open Journal of the Communications Society (OJ-COMS), *Computers and Electrical Engineering* (Elsevier), *Human-centric Computing and Information Sciences* (Springer), and the *Journal of Information Processing Systems*. He is a Guest Editor of Special Issues of IEEE Access, *Sensors*, IEEE/KICS Journal of Communications and Networks, and *Physical Communication*, and has served as a TPC Member for world-distinguished conferences, like the IEEE VTC, IEEE ICC, and IEEE PIMRC.

SONG NOH (Member, IEEE) received the B.S. degree in electrical engineering from Soongsil University, Seoul, South Korea, in 2008, the M.S. degree in electrical engineering from the Korea Advanced Institute of Science and Technology, Daejeon, South Korea, in 2010, and the Ph.D. degree in electrical and computer engineering from Purdue University, West Lafayette, IN, USA, in 2015. From 2015 to 2018, he was a System Engineer with the Next Generation and Standards Group, Intel Corporation, Hillsboro, OR, USA, and participated in the designing of the PHY/MAC layer protocol for millimeter-wave mobile broadband systems. Since 2018, he has been a Faculty of the Department of Information Telecommunication Engineering, Incheon National University, Incheon, South Korea. His research interests include the design and analysis of millimeter-wave communication systems and adaptive signal processing for wireless communications. He was a co-recipient of the Communication Theory Symposium Best Paper Award at the 2014 IEEE Global Communications Conference (Globecom).